On the stability of the vertically stratified state of a vapor–gas mixture between two parallel condensed phases

Shigeru TAKATA*, Takeshi SHIMADA† and Hideyuki MIZUNO†

*Department of Mechanical Engineering and Science & Advanced Research Institute of Fluid Science and Engineering, Kyoto University, Kyoto 606-8501, Japan
†Department of Aeronautics and Astronautics, Kyoto University, Kyoto 606-8501, Japan

Abstract. Behavior of a vapor–gas mixture between two parallel plane condensed phases under a constant gravity is investigated on the basis of the Hamel model equation. First, the problem is studied numerically by putting a spatially one-dimensional constraint. Then, by relaxing the constraint to a two-dimensional one, the stability of the one-dimensional vertically stratified states is investigated, again numerically. It is demonstrated that, for certain parameter settings, the stratified states are unstable and undergo a transition to another state with convection rolls. The range of parameter set of this transition is presented. The influence of temperature field on the observed transition is also discussed.

Keywords: Stability, Convection-roll, Double diffusion, Kinetic theory of gases
PACS: 51.10.+y, 47.45.-n, 47.45.Ab, 47.50.Gj,47.55.pd

INTRODUCTION

Consider a binary mixture of a vapor and a noncondensable gas in the gap between two parallel plane condensed phases of the vapor. When the temperatures of the surfaces are different from each other, the formation of a layer stratified normal to the bounding surfaces with a slow flow evaporating from one side and condensing on the other is expected in the gap . The present paper is concerned with the stability of those stratified states when the system is subject to a gravitational force in the direction normal to the bounding surfaces. Intuitively, setting the surface temperatures different causes the difference of the corresponding saturation pressures and results in forming a vertical concentration gradient in the gap. It may cause a distribution of mass density increasing with height, and the state with such distribution seems unstable to undergo a transition to another state. Such primitive consideration motivated us to perform the present work.

Research on the stability of gas flows in the framework of the kinetic theory was initiated by the pioneering work by Cercignani and Stefanov [1]; since then, a lot of works have been devoted to fundamental problems such as the Bénard problem, Taylor–Couette instability (see, for example, [1, 2, 3] and the references therein). To our best knowledge, however, studied so far are the problems for single component systems. The present work would be the first that discusses the stability problem peculiar to multicomponent systems.

PROBLEM AND BASIC FORMULATION

We consider a binary mixture of a vapor (say, species A) and a noncondensable gas (say, species B) between two parallel plane condensed phases of the vapor under the gravity $(0,-g,0)$ ($g>0$) (Fig. 1). The condensed phases are located at $X_2=\pm D/2$ with uniform constant temperatures $T_\pm$. The saturation pressures of the vapor (species A) at these temperatures are denoted by $p^{\mathrm{A}}_\pm$. We shall investigate the behavior of the mixture in the gap on the basis of the Hamel BGK-type model Boltzmann equation [4] for binary gas mixtures, with a special interest in the stability of the vertically stratified state of the mixture. On the surface of the condensed phase, we assume that vapor molecules obey the complete condensation condition, while noncondensable gas molecules do the diffuse reflection condition. Then, with symbolic use

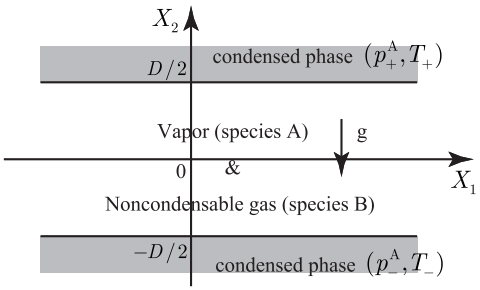

FIGURE 1. Schematic of the problem.

of Greek letters α and β for representing the component species, i.e., $\{\alpha,\beta\}=\{\mathrm{A},\mathrm{B}\}$, the problem is written by the equations

$$\frac{\partial f^\alpha}{\partial t}+\xi_i\frac{\partial f^\alpha}{\partial X_i}-g\frac{\partial f^\alpha}{\partial \xi_2}=K^{\mathrm{A}\alpha}n^{\mathrm{A}}(H^{\mathrm{A}\alpha}-f^\alpha)+K^{\mathrm{B}\alpha}n^{\mathrm{B}}(H^{\mathrm{B}\alpha}-f^\alpha), \tag{1a}$$

$$f^\alpha=\frac{\sigma_\pm^\alpha}{(2\pi/m^\alpha)^{3/2}(kT_\pm)^{5/2}}\exp\Big(-\frac{|\boldsymbol{\xi}|^2}{2kT_\pm/m^\alpha}\Big),\quad \xi_2\gtrless 0,\ X_2=\pm D/2, \tag{1b}$$

supplemented by initial data f_{in}^α. Here, f^α denotes the velocity distribution function of α species molecules, which is a function of time t, position $\boldsymbol{X}$ (or X_i), and molecular velocity $\boldsymbol{\xi}$ (or ξ_i); m^α the mass of a molecule of species α; k the Boltzmann constant; $K^{\beta\alpha}$'s some constants with symmetry $K^{\mathrm{AB}}=K^{\mathrm{BA}}$; and the other quantities are given as

$$H^{\beta\alpha}=\frac{n^\alpha}{(2\pi kT^{\beta\alpha}/m^\alpha)^{3/2}}\exp\Big(-\frac{|\boldsymbol{\xi}-\boldsymbol{v}^{\beta\alpha}|^2}{2kT^{\beta\alpha}/m^\alpha}\Big),\quad \sigma_\pm^{\mathrm{A}}=p_\pm^{\mathrm{A}},\quad \sigma_\pm^{\mathrm{B}}=\mp(2\pi kT_\pm m^{\mathrm{B}})^{1/2}\int_{\xi_2\lessgtr 0}\xi_2 f^{\mathrm{B}}d\xi_1d\xi_2d\xi_3,$$

$$\boldsymbol{v}^{\beta\alpha}=\frac{m^\beta\boldsymbol{v}^\beta+m^\alpha\boldsymbol{v}^\alpha}{m^\beta+m^\alpha},\quad T^{\beta\alpha}=T^\alpha+\frac{2m^\beta m^\alpha}{(m^\beta+m^\alpha)^2}\Big(T^\beta-T^\alpha+\frac{m^\beta}{6k}|\boldsymbol{v}^\beta-\boldsymbol{v}^\alpha|^2\Big),$$

with n^α, $\boldsymbol{v}^\alpha$, and T^α being the molecular number density, velocity, and *temperature* of the species α defined by

$$n^\alpha=\int f^\alpha d\xi_1d\xi_2d\xi_3,\quad \boldsymbol{v}^\alpha=\frac{1}{n^\alpha}\int\boldsymbol{\xi}f^\alpha d\xi_1d\xi_2d\xi_3,\quad T^\alpha=\frac{m^\alpha}{3kn^\alpha}\int|\boldsymbol{\xi}-\boldsymbol{v}^\alpha|^2f^\alpha d\xi_1d\xi_2d\xi_3,$$

where the integrations are over the whole $\boldsymbol{\xi}$ space.

Steady one-dimensional problem We first study the spatially one-dimensional steady problem: the problem (1) with $\partial/\partial t=\partial/\partial X_1=\partial/\partial X_3=0$. In this case, we need to specify the amount of noncondensable gas B or its average number density $n_{\mathrm{av}}^{\mathrm{B}}$ defined by $n_{\mathrm{av}}^{\mathrm{B}}=(1/D)\int_{-D/2}^{D/2}n^{\mathrm{B}}dX_2$, in place of the initial data f_{in}^α. Nondimensional reformulation shows that the problem is characterized by three parameters inherent in the molecular model: $m^{\mathrm{B}}/m^{\mathrm{A}}$, $K^{\mathrm{BA}}/K^{\mathrm{AA}}$, and $K^{\mathrm{BB}}/K^{\mathrm{AA}}$ and by other five parameters: $\mathrm{Kn}=\ell/D$ (the reference Knudsen number), $\mathrm{Fr}=(2kT_-/m^{\mathrm{A}})/Dg$ (the reference Froude number), T_+/T_-, $p_+^{\mathrm{A}}/p_-^{\mathrm{A}}$, and $n_{\mathrm{av}}^{\mathrm{B}}/n_-^{\mathrm{A}}$. Here ℓ is the reference mean-free-path of a molecule defined by $\ell=(8kT_-/\pi m^{\mathrm{A}})^{1/2}/(K^{\mathrm{AA}}n_-^{\mathrm{A}})$, and $n_-^{\mathrm{A}}=p_-^{\mathrm{A}}/kT_-$.

For spatially one-dimensional case, we can eliminate ξ_1 and ξ_3 from the system (1) by integrating it in ξ_1 and ξ_3 after multiplying 1 and $(\xi_1^2+\xi_3^2)^2$. This leads to the system for marginal distribution functions

$$g^\alpha(X_2,\xi_2)=\int_{-\infty}^{\infty}d\xi_1\int_{-\infty}^{\infty}d\xi_3\,f^\alpha(X_2,\boldsymbol{\xi}),\quad h^\alpha(X_2,\xi_2)=\int_{-\infty}^{\infty}d\xi_1\int_{-\infty}^{\infty}d\xi_3\,(\xi_1^2+\xi_3^2)\,f^\alpha(X_2,\boldsymbol{\xi}),$$

which we call system 1d, and we solve it numerically by the standard finite-difference method with the restriction of ξ_2 in a finite but sufficiently large interval $[-Z,Z]$. Outside this interval, g^α and h^α are assumed to vanish. In the actual computation, we set $Z/(2kT_-/m^{\mathrm{A}})^{1/2}=8$ and discretize the region $[-D/2,D/2]\times[-Z,Z]$ in $X_2\xi_2$-space by a nonuniform rectangular grid with 481×201 points symmetric with respect to 0 both in X_2 and ξ_2. The grid is coarser for smaller $|X_2|$ and for larger $|\xi_2|$. In the present problem, both g^α and h^α are discontinuous at $\xi_2=0$ at the top and bottom bounding surfaces, and the discontinuity propagates into the gas region along the characteristics of Eq. (1a) from the top bounding because of gravity. In the simulation code, we do not take into account the discontinuity, because it decreases exponentially along the characteristics in the scale of the molecular free path and the simulations are to be performed for small Knudsen numbers where the discontinuity and its influence are expected small.

Two-dimensional stability problem We next study the two-dimensional stability of the one-dimensional solution. To this end, we consider the mixture in a hypothetical two-dimensional square box as in [2], whose top and bottom are the same as those of the original problem. We assume that the left and right sides are specularly reflecting against both species of molecules (Fig. 2). Thus, we consider the problem (1) with $\partial/\partial X_3=0$ supplemented with the boundary conditions

$$f^\alpha(t,0,X_2,\xi_1,\xi_2,\xi_3)=f^\alpha(t,0,X_2,-\xi_1,\xi_2,\xi_3), \tag{2a}$$

$$f^\alpha(t,D,X_2,\xi_1,\xi_2,\xi_3)=f^\alpha(t,D,X_2,-\xi_1,\xi_2,\xi_3), \tag{2b}$$

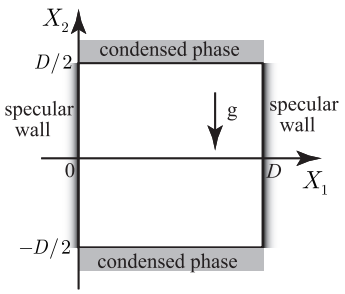

FIGURE 2. Schematic of the problem.

and initial data $f_{\rm in}^{\alpha}(X_1, X_2, \boldsymbol{\xi})$. This situation is considered in order to find a two-dimensional periodic solution with period $2D$ of the original problem. It is obvious that a one-dimensional solution of the original problem is also a solution of the present two-dimensional problem. We shall study the time evolution of the behavior of the mixture in the box from the initial data of the form

$$f_{\rm in}^{\alpha}(t=0, X_1, X_2, \boldsymbol{\xi}) = \frac{n_{\rm in}^{\alpha}(X_1, X_2)}{n_{\rm 1d}^{\alpha}(X_2)} f_{\rm 1d}^{\alpha}(X_2, \boldsymbol{\xi}), \quad n_{\rm in}^{\rm A} = n_{\rm 1d}^{\rm A} - \varepsilon\, n_{\rm 1d}^{\rm B} \cos(\pi X_1/D)\cos(\pi X_2/D), \quad n_{\rm in}^{\rm B} = n_{\rm 1d} - n_{\rm in}^{\rm A}, \tag{3}$$

where $n_{\rm 1d} = n_{\rm 1d}^{\rm A} + n_{\rm 1d}^{\rm B}$, $n_{\rm 1d}^{\alpha}$ the molecular number density of species α based on $f_{\rm 1d}^{\alpha}$, and ε a given (small) constant. The above initial data is a slightly disturbed one from the one-dimensional solution $f_{\rm 1d}^{\alpha}$ in such a way that the disturbance does not change the total amount of molecules of individual species in the box. Since we restrict the form of the initial data, the present problem is characterized by ε and the previous eight parameters $m^{\rm B}/m^{\rm A}$, $K^{\rm BA}/K^{\rm AA}$, $K^{\rm BB}/K^{\rm AA}$ Kn $= \ell/D$, Fr $= (2kT_-/m^{\rm A})/Dg$, T_+/T_-, $p_+^{\rm A}/p_-^{\rm A}$, and $n_{\rm av}^{\rm B}/n_-^{\rm A}$. Here $n_{\rm av}^{\rm B}$ should be interpreted as $n_{\rm av}^{\rm B} = (1/D^2)\int_{-D/2}^{D/2}\int_0^D n^{\rm B} dX_1 dX_2$.

In the time evolution, if the initial disturbance to one-dimensional solution grows and the state of the mixture in the box transforms to another state, we may assert that the one-dimensional solution is unstable in the original problem of Fig. 1. However, we cannot assert the reverse: going back to the undisturbed one-dimensional solution does not mean its (two-dimensional) stability in the original problem. It is because we have excluded, for instance, solutions with a period other than $2D$, nonsymmetric periodic solutions with the period $2D$, etc. and consider the time evolution only from a special type of initial data. What we can clarify in the present work is merely that the one-dimensional stratified state of the mixture in the gap schematized in Fig. 1 is unstable for the set of parameters for which we observe a transition to another state. Nevertheless, in the subsequent sections, we will abusively use the word "stable" when we do not observe a transition in our simulation. But, in the case, we shall use italic like *stable*.

For spatially two-dimensional case, we can eliminate ξ_3 from the system (1) – (3) by integrating it in ξ_3 after multiplying 1 and ξ_3^2. The resulting, which we call system 2d, is the system for marginal distribution functions

$$G^{\alpha}(t, X_1, X_2, \xi_1, \xi_2) = \int_{-\infty}^{\infty} f^{\alpha}(t, X_1, X_2, \boldsymbol{\xi})\, d\xi_3, \quad H^{\alpha}(t, X_1, X_2, \xi_1, \xi_2) = \int_{-\infty}^{\infty} \xi_3^2\, f^{\alpha}(t, X_1, X_2, \boldsymbol{\xi})\, d\xi_3,$$

and we solve it by the standard finite-difference method [2]. In our method, the terms of differentiation are evaluated by the explicit scheme and the collision integrals are from the data at the previous time step. We restrict $\xi_1\xi_2$-space in a finite but sufficiently large square region $[-Z, Z] \times [-Z, Z]$, and assume G^{α} and H^{α} to vanish outside this region. In the actual computation, we set $Z/(2kT_-/m^{\rm A})^{1/2} = 6$ and discretize the interval $[0, D]$ of X_1 uniformly and the rectangular parallelepiped region $[-D/2, D/2] \times [-Z, Z] \times [-Z, Z]$ of $X_2\xi_1\xi_2$-space nonuniformly but symmetric with respect to 0 in all of X_2, ξ_1, and ξ_2. The grid is coarser for smaller $|X_2|$ and for larger $|\xi_1|$ and $|\xi_2|$. The discontinuity inside the gas region is not taken into account again because the simulation is performed for small Knudsen numbers. Information about the grid system will be given later.

G^{α} and H^{α} corresponding to $f_{\rm 1d}^{\alpha}$, which is necessary to prepare the initial data, can be recovered from the data of macroscopic quantities $n_{\rm 1d}^{\alpha}$, $\boldsymbol{v}_{\rm 1d}^{\alpha}$, and $T_{\rm 1d}^{\alpha}$ for system 1d by numerically solving system 2d with $\partial/\partial t = \partial/\partial X_1 = 0$. In the recovering process, we use the same grid as that for system 1d in $X_2\xi_2$-space and that for system 2d in $X_1\xi_1$-space. The grid for system 2d in $X_2\xi_2$-space is a coarser sub-system of that for system 1d, and thus neither iteration nor interpolation is required in preparing the initial data.

RESULTS AND DISCUSSION

In numerical simulations, we fix the values of a part of parameters as $K^{\rm AB}/K^{\rm AA} = K^{\rm BB}/K^{\rm AA} = 1$, $m^{\rm B}/m^{\rm A} = 0.5$, and $n_{\rm av}^{\rm B}/n_-^{\rm A} = 4$ and mainly study the dependence of the issued behavior of the mixture on the remaining T_+/T_-, $p_+^{\rm A}/p_-^{\rm A}$, Kn, and Fr, especially on the last three. In the two-dimensional time-evolution problem, we always set $\varepsilon = 0.1$.

Main results: the case $T_+/T_- = 1$

Steady one-dimensional solution Simulations of system 1d are carried out for various values of $p_+^{\rm A}/p_-^{\rm A}(\geq 1)$ and Fr in the case of Kn $= 0.01$, 0.02, 0.03, 0.04, and 0.05. The obtained steady one-dimensional solutions, which show

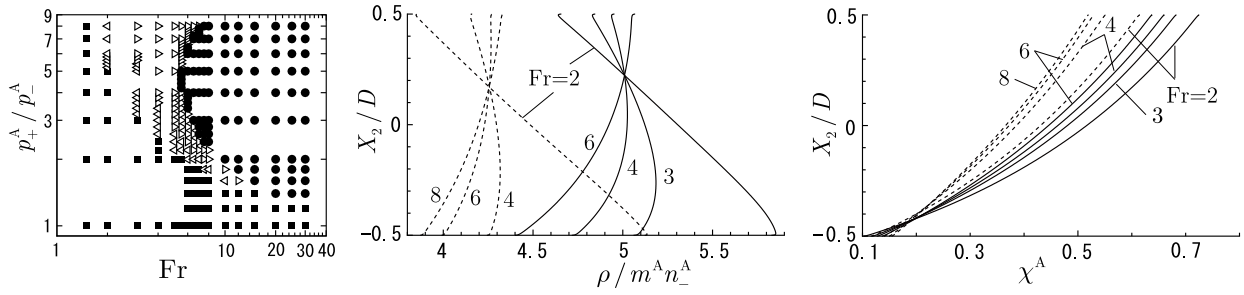

(a) Classification (b) $\rho / m^{\mathrm{A}} n_-^{\mathrm{A}}$ vs X_2 / D (c) χ^{A} vs X_2 / D

FIGURE 3. Classification of vertically stratified states in $(\mathrm{Fr}, p_+^{\mathrm{A}}/p_-^{\mathrm{A}})$-plane and some examples of the dimensionless mass density $\rho/m^{\mathrm{A}}n_-^{\mathrm{A}}$ and concentration χ^{A} profiles in the case of $\mathrm{Kn} = 0.03$. In (a), symbols ■, ◁, ▷, and ● indicate the states of type 1, 2, 3, and 4, respectively. In (b) and (c), solid lines indicate the profiles for $p_+^{\mathrm{A}}/p_-^{\mathrm{A}} = 4$ and dashed lines those for $p_+^{\mathrm{A}}/p_-^{\mathrm{A}} = 3$.

vertically stratified states, can be classified into four types: **[type 1]** mass density $\rho(X_2)$ of the mixture, which is defined by $\rho = m^{\mathrm{A}}n^{\mathrm{A}} + m^{\mathrm{B}}n^{\mathrm{B}}$, decreases monotonically with X_2 in the interval $|X_2/D| \le 0.45$; **[type 2]** ρ is not monotonic in X_2 in the above interval, i.e., it first increases, takes its maximum, and then decreases with X_2. In addition, it satisfies the inequality $\rho(-0.45D) > \rho(0.45D)$; **[type 3]** ρ behaves in the same way as type 2, except that $\rho(-0.45D) < \rho(0.45D)$. **[type 4]** ρ increases monotonically with X_2 in the interval $|X_2/D| \le 0.45$. Figure 3(a) shows the classification of the obtained vertically stratified states in $(\mathrm{Fr}, p_+^{\mathrm{A}}/p_-^{\mathrm{A}})$-plane for $\mathrm{Kn} = 0.03$; and Figs. 3(b) and (c) show, respectively, examples of mass density and concentration profiles in the case of $\mathrm{Kn} = 0.03$. In (b) and (c), the solid lines indicate the profiles for $\mathrm{Fr} = 2$, 3, 4, and 6 in the case of $p_+^{\mathrm{A}}/p_-^{\mathrm{A}} = 4$, while the dashed lines those for $\mathrm{Fr} = 2$, 4, 6, and 8 in the case of $p_+^{\mathrm{A}}/p_-^{\mathrm{A}} = 3$. State classification map is almost identical among the examined five different values of Kn.

Because of the density profile, one might intuitively think that the state would become less stable for larger label number of state (for instance, type 4 would be less stable than type 1). However, as will be demonstrated later, it is not necessarily true, and it can happen that the state "type 1" is less *stable* than the "type 4."

Two-dimensional time evolution Simulations of system 2d are carried out for various values of $p_+^{\mathrm{A}}/p_-^{\mathrm{A}}$ and Fr in the case of $\mathrm{Kn} = 0.02$, 0.03, and 0.05. We observed that (I) the disturbance to the vertically stratified state tends to vanish, and finally the undisturbed vertically stratified state is recovered — what we abusively call *stable*; or that (II) the disturbance to the vertically stratified state grows, and finally a steady state with one convection roll is established in the box — what we call unstable. Figures 4 and 5 show two examples of mass density ρ, concentration χ^{A}, and (momentum-based) flow velocity $\boldsymbol{v}$, defined by $\boldsymbol{v} = (m^{\mathrm{A}}n^{\mathrm{A}}\boldsymbol{v}^{\mathrm{A}} + m^{\mathrm{B}}n^{\mathrm{B}}\boldsymbol{v}^{\mathrm{B}})/\rho$, at a final steady state with one convection roll. Figure 6 shows the classification of those final states in $(\mathrm{Fr}, p_+^{\mathrm{A}}/p_-^{\mathrm{A}})$-plane that are obtained after the time evolution. It demonstrates that (i) vertically stratified states become unstable as $p_+^{\mathrm{A}}/p_-^{\mathrm{A}}$ increases, (ii) there is the

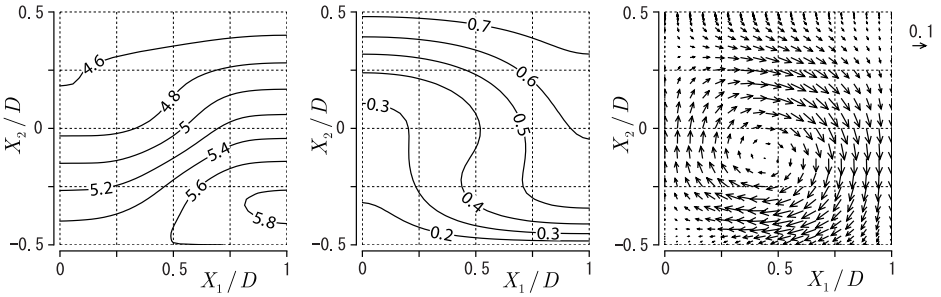

(a) Contour plots of $\rho / m^{\mathrm{A}} n_-^{\mathrm{A}}$ (b) Contour plots of χ^{A} (c) $\boldsymbol{v}/(2kT_-/m^{\mathrm{A}})^{1/2}$

FIGURE 4. Dimensionless mass density $\rho/m^{\mathrm{A}}n_-^{\mathrm{A}}$, concentration χ^{A}, and dimensionless flow velocity $\boldsymbol{v}/(2kT_-/m^{\mathrm{A}})^{1/2}$ at the final steady state with one convection roll in the case of $\mathrm{Kn} = 0.03$, $\mathrm{Fr} = 2$, and $p_+^{\mathrm{A}}/p_-^{\mathrm{A}} = 4$. In (c), the arrows indicate $\boldsymbol{v}/(2kT_-/m^{\mathrm{A}})^{1/2}$ at their starting points. They are drawn every two grid points both in X_1 and X_2 directions. The reference length of the arrows is shown on the top right corner.

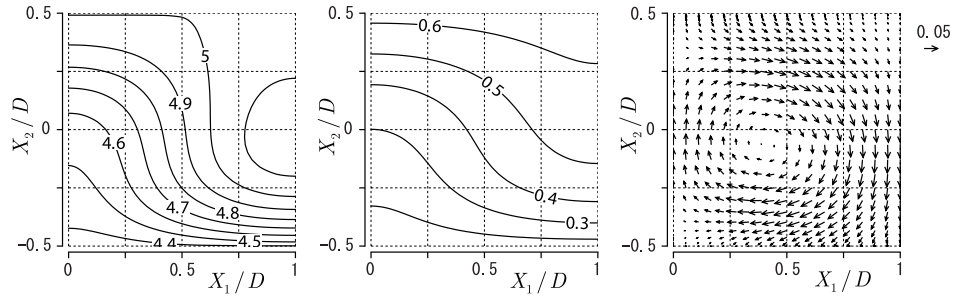

(a) Contour plots of $\rho/m^{\mathrm{A}}n_{-}^{\mathrm{A}}$ (b) Contour plots of χ^{A} (c) $\boldsymbol{v}/(2kT_{-}/m^{\mathrm{A}})^{1/2}$

FIGURE 5. Dimensionless mass density $\rho/m^{\mathrm{A}}n_{-}^{\mathrm{A}}$, concentration χ^{A}, and dimensionless flow velocity $\boldsymbol{v}/(2kT_{-}/m^{\mathrm{A}})^{1/2}$ at the final steady state with one convection roll in the case of Kn $= 0.03$, Fr $= 6$, and $p_{+}^{\mathrm{A}}/p_{-}^{\mathrm{A}} = 4$. See the caption of Fig. 4. Here, in (c), the arrows are drawn every four grid points in X_1 direction and every two points in X_2 direction.

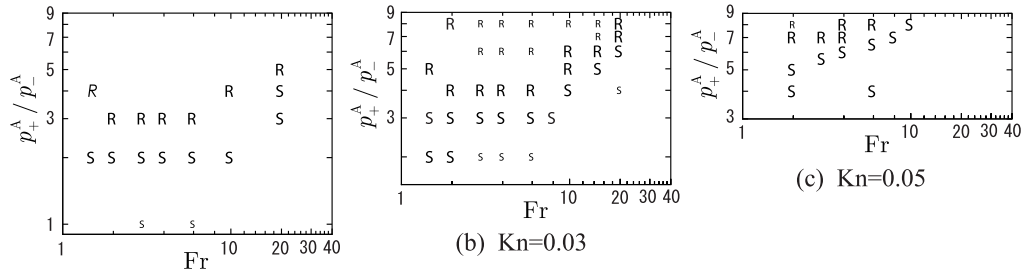

(a) Kn=0.02 (b) Kn=0.03 (c) Kn=0.05

FIGURE 6. Classification of the final states in the square box. (a) Kn $= 0.02$, (b) Kn $= 0.03$, and (c) Kn $= 0.05$. Symbol R indicates a steady state with one convection roll and S the undisturbed vertically stratified state. See the second paragraph on this page for the difference among roman R and S, small roman ʀ and s, and italic *R*.

same tendency as Kn decreases, and (iii) the classification of vertically stratified states does not provide a clear insight on their *stability*. For instance, the vertically stratified states in Fig. 3(b) for $p_{+}^{\mathrm{A}}/p_{-}^{\mathrm{A}} = 3$ are all recovered, while those for $p_{+}^{\mathrm{A}}/p_{-}^{\mathrm{A}} = 4$ all transform to another state with one convection roll. The feature (ii) is the same as that reported in the existing studies on the stability problems such as the Bénard convection, Taylor–Couette flow, etc. [1, 2, 3]

We shall remark here that a fake solution may be observed in the simulation, if the grid is not fine enough. In fact, in preliminary simulations with coarser grids, we observed, for some parameter settings, those transitions to a steady state with two convection rolls in the square, to a oscillatory state with one convection roll or two convection rolls, etc., that vanished in the simulations with finer grids. In the present work, used as the standard is the grid with 37×49 points in the square ($0 \le X_1 \le D$, $-D/2 \le X_2 \le D/2$) and 41×81 points in the truncated $\xi_1\xi_2$-space with $Z/(2kT_{-}/m^{\mathrm{A}})^{1/2} = 6$. The time interval Δt is $\Delta t(2kT_{-}/m^{\mathrm{A}})^{1/2}/D = \mathrm{Kn} \times 10^{-1}$. We carried out simulations not only with the standard grid but also with doubled (or tripled, ..., if necessary) grids in one of X_1, X_2, ξ_1, and ξ_2 directions, and judged the simulation results to be reliable if the difference of the obtained molecular number densities, pressures, and temperatures does not exceed relatively 5 % during the whole time evolution. When this criteria was not fulfilled, we took the same procedure for the simulation with one of the finer grids until the same criteria is fulfilled against this new standard. Normal size roman R and S in Fig. 6 show the results that fulfill such criteria. The above confirmation process is crucial, especially for parameter settings near the boundary between the R and S regions. Nevertheless, in Fig. 6, we also indicate by small roman R and S the results of simulations with the standard grid, for which the above grid test has not been made. From experience, we consider these results also reliable. Italic *R* for $p_{+}^{\mathrm{A}}/p_{-}^{\mathrm{A}} = 4$ and Fr $= 1.5$ in Fig. 6 means that the result does not meet the 5 % criteria but meet a slightly loosen criteria of 5.8 %. In this case, we observed an anticlockwise convection roll as the final state, whereas we observed clockwise ones for the others.

Thermal stabilizing effect: the case $T_+/T_- = 1.1$

Up to this point, in numerical simulations, we have restricted ourselves to the case $T_+/T_- = 1$. Physically, the saturation pressure of a vapor depends on temperature because of the Clausius–Clapeyron relation, and thus $p_+^{\mathrm{A}}/p_-^{\mathrm{A}}$ is not a parameter independent of T_+/T_-. The previous parameter setting, i.e., $p_+^{\mathrm{A}}/p_-^{\mathrm{A}} \geq 1$ but $T_+/T_- = 1$, is an idealization of the fact that the saturation pressure is, in general, a rapidly increasing function of temperature. A physically natural setting of temperature for $p_+^{\mathrm{A}} > p_-^{\mathrm{A}}$ is $T_+ > T_-$; and it would be relevant to study the stability for this parameter setting, because higher temperature at the top might stabilize the vertically stratified state enough to completely suppress the transitions to another state observed in the previous subsection. We carried out simulations for several values of Fr and $p_+^{\mathrm{A}}/p_-^{\mathrm{A}}(>1)$ in the case of $T_+/T_- = 1.1$ and $\mathrm{Kn} = 0.03$. Figures 7 and 8 show the results, which demonstrate that the expected stabilization effect does exist but is not strong enough to completely suppress the transition observed before. To be more precise, (i) in a certain range of the parameter set, the steady vertically stratified state is unstable and a transition to a two-dimensional steady state with one convection roll takes place; (ii) this parameter range is, however, smaller than that for $T_+/T_- = 1$. The classification of the observed final states is shown in Fig. 7, and an example of those states with one convection roll is in Fig. 8. We also carried out preliminary simulations with the standard grid for $T_+/T_- \geq 1.2$ in the parameter range in Fig. 7(b). The results suggest a rapid increase of the thermal stabilizing effect: we did not observe a transition from a vertically stratified state to another.

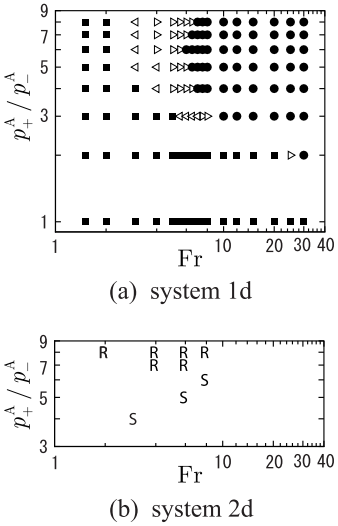

FIGURE 7. Classification of the states in the case of $T_+/T_- = 1.1$ and $\mathrm{Kn} = 0.03$. (a) System 1d. (b) System 2d. See the caption of Fig. 3 for (a) and that of Fig. 6 for (b).

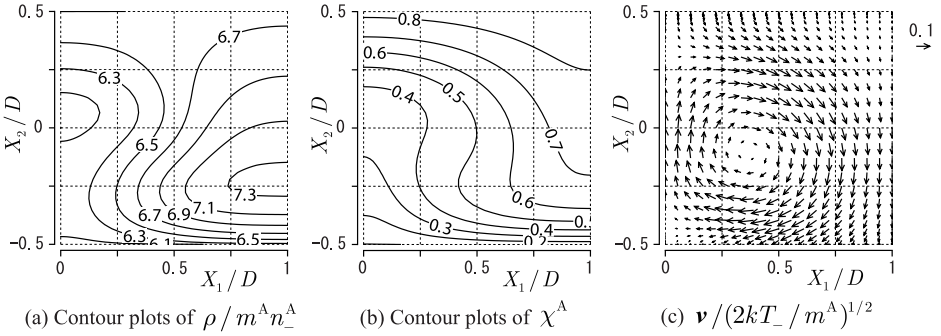

FIGURE 8. Dimensionless mass density $\rho/m^{\mathrm{A}}n_-^{\mathrm{A}}$, concentration χ^{A}, and dimensionless flow velocity $\boldsymbol{v}/(2kT_-/m^{\mathrm{A}})^{1/2}$ at the final steady state with one convection roll in the case of $\mathrm{Kn} = 0.03$, $\mathrm{Fr} = 4$, $p_+^{\mathrm{A}}/p_-^{\mathrm{A}} = 7$, and $T_+/T_- = 1.1$. See the caption of Fig. 5.

Acknowledgments The authors thank Professor Kazuo Aoki for his interest in this work and Mr. Hiroyasu Shimizu for his help in performing a part of simulations. This work is supported by the grant-in-aid (No. 15760108) for Scientific Research from the JSPS and by the COE program of the MEXT for Research and Education on Complex Functional Mechanical Systems.

REFERENCES

1. Cercignani, C., Stefanov, S., *Transp. Theory Stat. Phys.*, **21**, 371-381 (1992); Stefanov, S., Cercignani, C., *Eur. J. Mech. B/Fluids*, **11**, 543-554 (1992).
2. Sone, Y., Aoki, K., Sugimoto, H., *Phys. Fluids*, **9**, 3898-3914, 1997.
3. Sone, Y., Aoki, K., Sugimoto, H., Motohashi, M., in *RGD*, edited by Harvey, J. and Lord, G., Oxford Univ. Press, Oxford, 1995, pp. 135-141; Stefanov, S., Cercignani, C., *J. Fluid Mech.*, **256**, 199-213 (1993); Riechelmann, D., Nanbu, K., *Phys. Fluids*, A**5**, 2585-2587 (1993); Yoshida, H., Aoki, K., in *RGD*, edited by Capitelli, M., AIP, New York, 2005, pp. 467-472; Stefanov, S., Roussinov, V.M., Cercignani, C., in *RGD*, edited by Capitelli, M., AIP, New York, 2005, pp. 529-534.
4. Hamel, B. B., *Phys. Fluids*, **8**, 418-425 (1965).